MATERIALS SCIENCE

Programmable self-propelling actuators enabled by a dynamic helical medium

Ling-Ling Ma†, Chao Liu†, Sai-Bo Wu, Peng Chen, Quan-Ming Chen, Jia-Xin Qian, Shi-Jun Ge, Yuan-Hang Wu, Wei Hu*, Yan-Qing Lu*

Rotation-translation conversion is a popular way to achieve power transmission in machinery, but it is rarely selected by nature. One unique case is that of bacteria swimming, which is based on the collective reorganization and rotation of flagella. Here, we mimic such motion using the light-driven evolution of a self-organized periodic arch pattern. The range and direction of translation are altered by separately varying the alignment period and the stimulating photon energy. Programmable self-propelling actuators are realized via a specific molecular assembly within a photoresponsive cholesteric medium. Through rationally presetting alignments, parallel transports of microspheres in customized trajectories are demonstrated, including convergence, divergence, gathering, and orbital revolution. This work extends the understanding of the rotation-translation conversion performed in an exquisitely self-organized system and may inspire future designs for functional materials and intelligent robotics.

INTRODUCTION

Motions—including translations, rotations, swings, vibrations, etc.—are ubiquitous in the world (*1*). Rotation-translation conversion has kept being an unfailing paradigm for the energy transduction in artificial systems. For instance, the back-and-forth translation of an engine's piston to rotate wheels and then to the translation of vehicles. However, this dominant conversion mode is rarely selected by nature. Bacteria can swim freely in liquids by using flagella (*2*, *3*). Here, the protein flagellar motor is driven by the transmembrane flux of H^+ or Na^+, promoting the collective reorganization and rotation of flagella. It works similar to screw propellers driven by tiny rotary motors. Notably, in addition to the molecular motor, the mechanical gear system is replaced by self-assembled microstructures. This kind of motion is unique, and no counterpart has ever been found in advanced beings. If one can mimic such stimuli responsiveness and microstructure-engaged motions with an active bottom-up self-organized composite, then versatile self-propelling microactuators would be created, enabling accurate, nonmechanical, and even programmable rotation-translation conversions. It will inspire new intelligent devices such as robots, assembly lines, and automatic sorters operating in mesoscope or microcosm.

In the natural world, organisms move based on the collective contraction of muscle tissues triggered by neuronal signals. To mimic the functionality of muscles, various smart materials with the ability to perceive external stimuli have been developed (*4*–*6*). Liquid crystal (LC) polymers can simulate motions—such as oscillating (*7*, *8*), rotating (*9*), and creeping (*10*)—by specifically bending or twisting the films. These deformations originate from the complex asymmetric contraction or expansion on the opposite sides (*11*–*13*) via presetting designed director configuration with specific external stimulation. In addition to solid films, LC, an ordered anisotropic medium exhibiting stimuli-responsive fluidic flow (*14*–*17*) and elastic deformation (*18*–*21*), supplies another platform for liquid actuators (*22*–*25*). Doped with a certain amount of light-driven molecular motor, the cholesteric LC (CLC) exhibits a reversibly tunable helical pitch *p*. Winding and unwinding processes can be separately carried out under the light stimulation with different photon energies. Moreover, through properly selecting the molecular motor and rationally setting the stimulating condition, the orientation of helical axis can be three-dimensionally manipulated (*26*). For a semi-free CLC film, a fingerprint texture is formed because of the fluctuated helical structure adjacent to the LC-air interface (*27*, *28*). Along with winding/unwinding, the torque induced by the variation of intrinsic viscoelasticity triggers the rotation of microparticles (*27*, *29*, *30*). It provides a perfect counterpart for above protein motors. So far, the engineering of self-organized microstructure-engaged transmission systems is still elusive, hindering the emergence of programmable self-propelling actuators.

Here, we propose a strategy for such self-propelling actuators via architecting an exquisite configuration in a photoresponsive helical medium. The light-driven motor is enabled by the winding/unwinding of CLC helixes derived from the photoinduced conformational change of the doped chiral molecular switches. The rotation-translation conversion is accomplished by introducing a periodically and continuously varied alignment. In addition, the direction of in-plane translation can be rationally designed via preprogramming the alignment condition. For the proof-of-principle demonstration of programmable actuators, we adopt microspheres to verify their converging, diverging, aggregating, and orbiting functions. This work mimics the motion of bacteria and demonstrates the functions of programmable self-propelling actuators.

RESULTS

Light-driven dynamics of helical structures

When coated onto a unidirectional planar alignment layer, as presented in Fig. 1A, the CLCs adjacent to the substrate (green rods) are guided by the alignment agent (yellow rods parallel to the *y* axis). Planar helical layers with standing helixes (along the *z* axis) develop from the substrate and occupy the bulk of the film. The handedness of the helical structure is determined by the chirality of the dopant. The helical pitch of CLC is defined in Fig. 1A, depending on both the helical twisting power (HTP) and the concentration of the chiral

National Laboratory of Solid State Microstructures, College of Engineering and Applied Sciences, Nanjing University, Nanjing 210093, China.
*Corresponding author. Email: huwei@nju.edu.cn (W.H.); yqlu@nju.edu.cn (Y.-Q.L.)
†These authors contributed equally to this work.

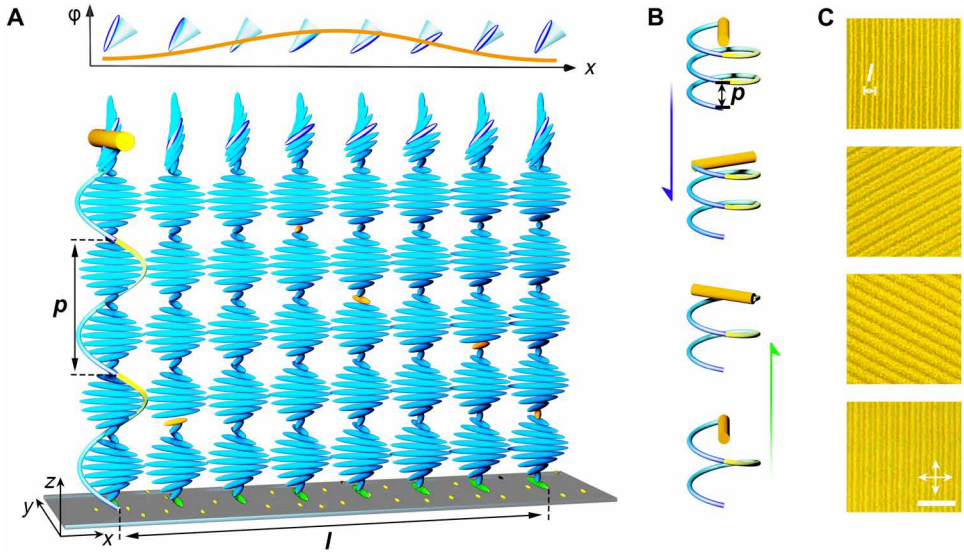

Fig. 1. Unidirectionally aligned semi-free CLC. (**A**) Helical configuration of the semi-free film (bottom) and corresponding fluctuated phase profile (top). *l* denotes the stripe period, and *p* indicates the helical pitch. (**B**) Schematic illustrations of the light-stimulated winding/unwinding of CLC helixes. Blue and green half-headed arrows denote the light stimulation conditions. Orange cylinders in (A) and (B) denote the directions of grating stripes. (**C**) Grating textures corresponding to the states shown in (B). White arrows denote the polarizer and analyzer transmission axes, respectively. Scale bar, 20 μm.

dopant. Because of the air-induced homeotropic anchoring, a lateral periodic director fluctuation is generated near the LC-air interface under the antagonistic anchoring condition (text S1). A periodic variation of phase φ occurs as a result of the repeatable director undulation (mazarine rods) in the length of *l*. *l* is typically several times larger than *p*, and it is a feature of the equilibrium state with minimum free energy under given surface anchoring energy, elastic torque of the LC and HTP of the chiral dopant. Under a polarizing optical microscope (POM), a grating with the period of *l* is observed. Notably, the grating vector is free with respect to the alignment (*y* axis), and it is determined by both the film thickness and the helicity of CLC for a given alignment (fig. S1). Here, the grating vector along the *x* axis is just for easy illustration. In this work, a photoresponsive left-handed chiral dopant ChAD-3c-S (orange rods) is adopted. When the film is exposed to blue light (450 to 490 nm), continuous unwinding occurs because of the change of molecular conformation (Fig. 1B), resulting in a gradual increase of *p* (fig. S2). The inverse winding process can be triggered by the green light irradiation (fig. S2) or at high temperature. Figure 1C vividly reveals the synchronous rotation of the grating with the winding/unwinding of the CLC. Thanks to the anisotropic viscoelasticity of LC, the collective in-plane rotation of LC directors provides a rotation torque to suspended particles, thus supplying a self-organized light-driven motor (*27*, *29*).

Self-organized microstructure engaged rotation-translation conversion

Since the optical and elastic anisotropies are both dependent on the director field, the rotation-translation conversion could be reasonably expected by rationally programming the director distribution of LC. The initial orientations of helixes follow the guidance of local alignments; thus, they can be spatially manipulated via photopatterning (Fig. 2A). Here, a periodically and continuously varied alignment is introduced. Its orientation is expressed as

$$n = (n_x, n_y, n_z) = (\cos\alpha, \sin\alpha, 0) \quad (1)$$

where the azimuthal angle $\alpha = \pi x/\Lambda$ or $-\pi x/\Lambda$, and Λ is the alignment period. Figure 2B illustrates the alignment for $\alpha = \pi x/\Lambda$, which is composed of alternate splay and bend orientations along *x*. Because of the fixed angle between the grating vector and the corresponding alignment for a given CLC film, the generated grating stripes splay and bend accordingly and form a periodic arch pattern (Fig. 2C). The period of the arch pattern equals to Λ, which is 100 μm in our experiments. Forked edge dislocations (*31*) with Burger's vector of *l* tend to exist in splay regions of the periodic arch pattern (Fig. 2C and fig. S3). The periodicity of their distribution perfectly matches with Λ. Under blue light exposure, collective unwinding occurs, resulting in a gradual increase of *l* (Fig. 2D). After 15 min, *l* approaches the maximum. This variation reflects the light-driven structure evolution. To further inspect the order of the periodic arch pattern, diffraction patterns are recorded, as shown in Fig. 2E. Diffraction rings are observed because of the continuous curving of the grating vector and the uniform *l*. Along with blue light exposure, the radius and intensity of the diffraction ring decrease, which results from the increase of *l* and the order decay, respectively.

Now, let us focus on a single period of the pattern with the local tangential directions of the grating stripes labeled by a group of blue bars. Along with the unwinding of the helix, blue bars rotate locally, i.e., no flow occurs (text S2), giving a directional shift of the periodic arch pattern and corresponding dislocations along $-x$ (Fig. 2F and movie S1). The dependency of *x*-direction displacement Δx on the rotation angle θ of the grating is presented in Fig. 2G. It is obvious that the pattern shifts one Λ when the helix unwinds each half pitch. The unwinding process of CLC is thus successfully transformed to the lateral shift of the periodic arch pattern and the translation speed is proportional to Λ, showing a Λ-determined velocity (fig. S4). Furthermore, if the alignment pattern is set as $\alpha = -\pi x/L$, then the pattern shifts in the opposite direction (fig. S5). The shift

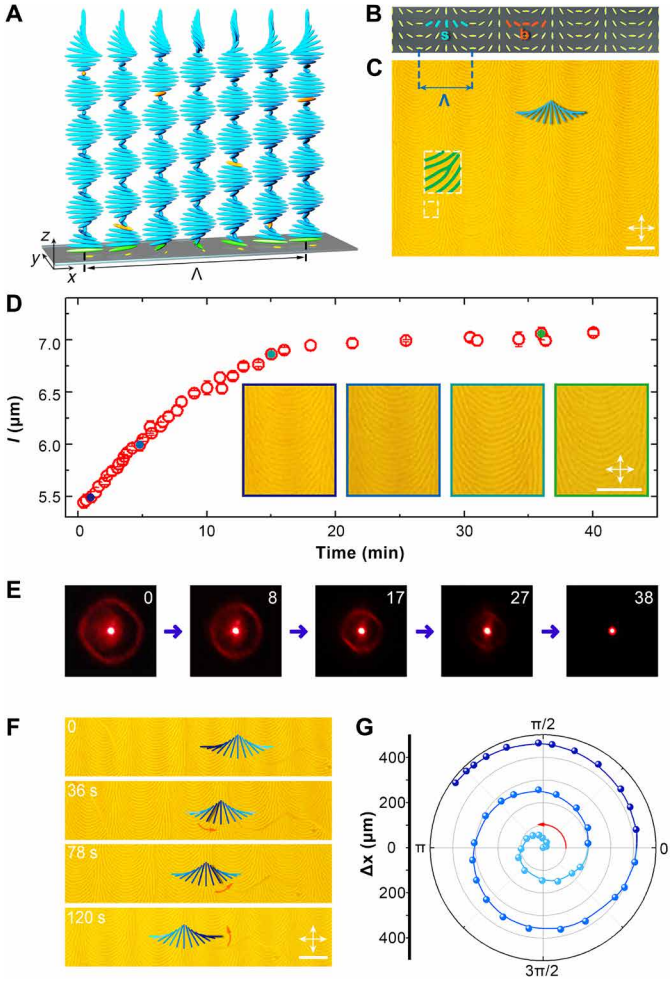

Fig. 2. Light-stimulated evolutions of photopatterned textures. (**A**) Helical configuration of the photopatterned CLC. (**B**) Schematic of the alignment condition. (**C**) POM texture of the generated periodic arch pattern. The group of blue bars denotes the local tangential directions of grating stripes in a single period. The inset illustrates a magnified texture with an edge dislocation. (**D**) Relationship between *l* and the exposure time. Insets are POM images of periodic arch patterns with different *l* during blue light exposure. The irradiance of blue light is about 100 μW/cm^2. (**E**) Diffraction patterns during the exposure with exposure time labeled (min). (**F**) Light-stimulated shift of the periodic arch pattern. The exposure time is labeled in corresponding micrographs. (**G**) Dependency of Δ*x* on θ. White arrows denote the polarizer and analyzer transmission axes, respectively. Scale bars, 50 μm.

direction can be reversed by changing the wavelength of stimulating light as well.

The texture vividly reveals the specific spatial director field of the CLC. Actually, besides optical anisotropy, other properties, such as elasticity, are also bonded to the director field (*32*–*34*). The light-driven lateral shift of the periodic arch pattern is expected to provide a thrust arising from the unidirectional moving of the periodically varied elasticity. Here, 3-μm-diameter microspheres with weak tangential anchoring are sputtered on the film to verify the propulsion. They are partially embedded in the CLC film, as observed under the confocal microscope (fig. S6). Most microspheres (~80%) are trapped by dislocations, which facilitates the reduction of free energy of the system (*35*). A schematic is drawn to present the surrounding director field of the partially embedded microsphere (fig. S7). As revealed in Fig. 3A and movie S2, they are carried by dislocations and transported along with the shift of periodic arch pattern. In our work, an optimized irradiance of 100 μW/cm^2 is selected to achieve steady and predictable motions of microspheres (fig. S8A). The trajectories and moving speed of three dislocation-trapped microspheres are analyzed and presented in Fig. 3B and fig. S8B. Motions of microspheres are synchronous to the lateral shift (−*x*) of the pattern within the first 25 min and exhibit excellent directional selectivity, with Δ*y* 20 times smaller than Δ*x*. Then, microspheres cannot keep pace with the shift of the periodic arch pattern, attributing to the elasticity-induced decreasing of driving force after long-time exposure. Considering the interaction between microspheres and dislocations, a series of potential wells exist along *x*, and microspheres are more probably trapped in the potential wells (Fig. 3C, i). *U* and *P* denote the potential and probability, respectively. When the periodic arch pattern is shifted under the light stimulation, the potential wells move accordingly. The mismatches between pairs of potential wells and microspheres result in a sufficient elastic driving force (Fig. 3C, ii), leading to the −*x* transportations of microspheres (Fig. 3C, iii).

To support the mobility, the elastic driving force F_e should overcome the Stokes drag force $F_s = 6\pi\eta Rv$ (*36*), where η is the viscosity of the fluid, *R* is the sphere radius, and *v* is the speed. Here, η = 29.9 mPa·s and *R* = 1.5 μm. Thus, F_s is about 0.2 pN at *v* = 15 μm/min, and F_s is about 1.0 pN at *v* = 68 μm/min, which is the maximum *v*. The elastic energy density of the CLC film is mainly determined by the helical structure with the characteristic of the helical pitch (*37*). F_e originates from the elastic energy density change Δ*f* during the light-induced variation of *p* (from $p_0 \approx 2$ μm to $p_1 \approx 4$ μm within the first 80 min; fig. S2)

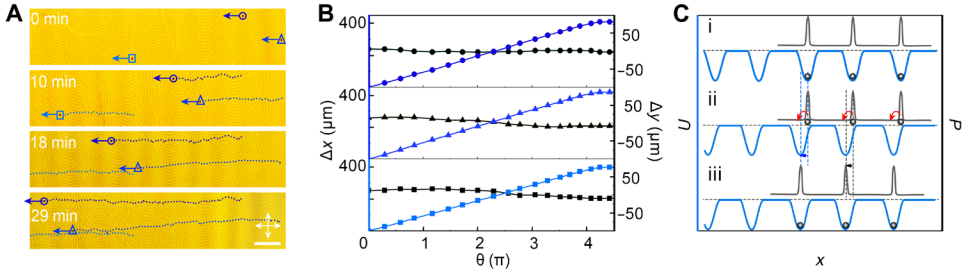

Fig. 3. Microstructure-engaged rotation-translation conversion. (**A**) Transport of microspheres toward −*x*. White arrows denote the polarizer and analyzer transmission axes, respectively. The exposure time is labeled in corresponding micrographs. Scale bar, 50 μm. (**B**) Dependencies of Δ*x* (blue) and Δ*y* (black) on θ. (**C**) Spatial potential analysis on light-driven transportations of microspheres.

$$\Delta f \approx \frac{1}{2} \cdot K_{22} \cdot 4\pi^2 \cdot \frac{p_1^2 - p_0^2}{p_1^2 \cdot p_0^2} \quad (2)$$

where $K_{22} \approx 5$ pN is the twist elastic constant. The power is calculated as

$$P = \Delta f \cdot V/t \quad (3)$$

where $V = \frac{4}{3}\pi R^3$ and $t = 80$ min. $F_e = P/v \approx 0.2$ pN at $v \approx 15$ μm/min. Thus, F_e equals to F_s, suggesting an elasticity change mechanism for motions of particles. In our work, particles tend to be trapped and carried by dislocations. The shift of dislocations is induced by the variation of free energy during the structure evolution, which is similar to the case of the CLC filled in a Grandjean-Cano wedge (*31*). Here, the antagonistic anchoring and the periodically variant surface alignment lead to complex curvatures of helical axes and irregular relaxations of the helical pitches (fig. S6A). Fortunately, the trapping and moving mechanism makes the picture of rotation-translation conversion easy to be caught (fig. S9).

Programmable self-propelling actuators

The light-driven winding/unwinding of CLC helix is successfully converted to the translation of microspheres. The translation follows the direction of periodic alignment changing. This suggests that programmable self-propelling actuators can be realized via rationally presetting the alignment condition. As shown in Fig. 4 (A and B, i), radial periodic alignments with $\alpha = \pi r/\Lambda$ and $-\pi r/\Lambda$ are carried out separately, where r is the polar radius. Accordingly, periodic circular arch patterns with opposite orientations are formed. Under the stimulation of blue light, uniformly scattered microspheres converge to and diverge from the center, respectively (Fig. 4, A and B, ii to iv; fig. S10; and movies S3 and S4). If we combine these two designs, then microspheres will aggregate at the green circle–labeled boundary (Fig. 4C, fig. S10, and movie S5). In addition to the linear transport, orbital translation is achieved by presetting an azimuthally continuously varied alignment pattern (Fig. 4D and movie S6). A reversible process is observed under green light irradiation (fig. S11). The above functions of self-propelling actuators are inherently encoded in their patterned structures, which is expected to be freely tailored. It needs to be noticed that all birefringent colors, which are very sensitive to the film thickness,

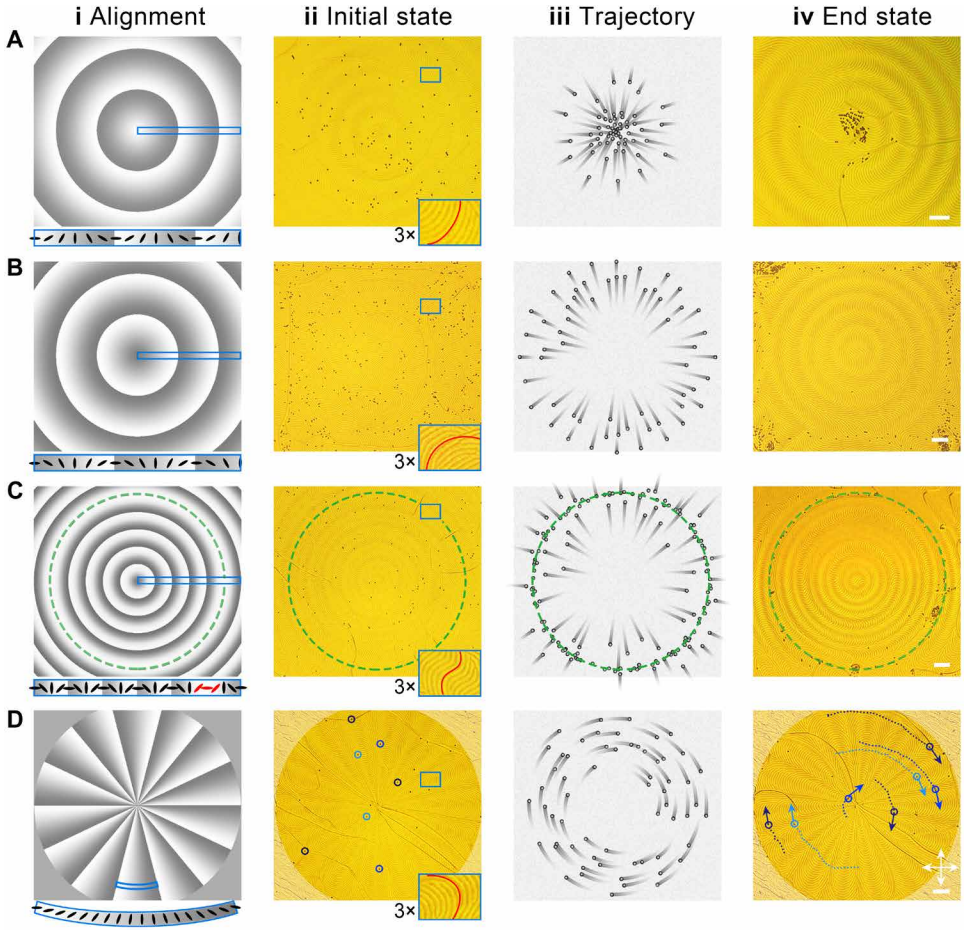

Fig. 4. Programmable transporting actuators. (i) Photoalignment conditions, (ii) initial states, (iii) trajectories, and (iv) end states of dispersed microspheres for motions of (**A**) converging, (**B**) diverging, (**C**) aggregating, and (**D**) orbiting. Insets in (ii) show the amplified images of the blue rectangular marked regions. The color change from white to gray indicates the alignment direction changing from 0° to 180°. The color difference of circles in (D) (ii and iv) is to distinguish microspheres. White arrows denote the polarizer and analyzer transmission axes, respectively. Scale bars, 50 μm.

keep uniform under irradiation, indicating that no flow occurs during the winding/unwinding of the helical structure (text S2).

DISCUSSION

So far, we have realized the rotation-translation conversion within a light-driven and microstructure-engaged transmission system. By presetting a periodically and continuously varied alignment, a periodic arch pattern is induced by the intrinsic self-assembly of CLC. The shift of the pattern under irradiation reflects the collective and continuous reorganization of the LC directors with fixed positions, similar to the rotation of the CLC grating (*30*). In this case, dislocations follow the shift of the periodic arch pattern and carry the particles synchronously (fig. S9). Thereby, it successfully converts the light-driven winding/unwinding of CLC helix to the unidirectional translation of microspheres. Film thickness is a key parameter for the self-propelling actuator. It can be tuned by the spin-coating rate. In our work, an optimized thickness of 8.7 μm (spin-coating rate of 1000 rpm) is selected (text S3). The range of translation displacement can be changed by varying the alignment period, while the translation direction follows the direction of the periodic alignment changing. Benefiting from the high-resolution and arbitrary surface pattern engineering of photoalignment, self-propelling actuators with customized trajectories can be generated by rationally presetting the alignment condition. Thus, it provides an excellent platform for programmable transmission systems. The chiral dopant endows the self-propelling actuators with reversible translations, which can be altered by the photoenergy. Moreover, the light stimulation is a remote control that only needs low-power light-emitting diodes (LEDs). The power density is only ~100 $\mu W/cm^2$, which is about 1/500 of the irradiance of optical tweezers (*38*), greatly reducing the light damage to the sample. Via introducing structured light irradiation and multivariant stimulations, dynamic switch among different trajectories is also achievable.

Thousands of particles are massively and parallelly transported in a single square millimeter. Besides 3-μm-diameter methacrylate-resin microspheres, other sized microspheres with diameters of 1.5, 5, 6.9, and 7.7 μm are also investigated. The mobilities of the first three types of microspheres are almost the same, except for reduced translational distances for larger microspheres. For 7.7-μm-diameter microspheres, they change the surrounding film thickness and distort the vectors of CLC gratings (fig. S12A), thus hindering the particle mobility. Microrods with the aspect ratio from 2 to 6 can be transported if the particle size is appropriate. Large microrods induce distortions similar to the case of 7.7-μm-diameter microspheres (fig. S12B). Other functional objects—such as bacteria, fluorescent and magnetic particles with proper size, shape, and anchoring condition—are expected to be transported as well. The maximum translation distance is >600 μm in our experiments, which can be further extended by increasing Λ, the concentration of the chiral molecular switch, or the film thickness. Thanks to the intrinsic fluidity and external field responsiveness of CLC, three-dimensional manipulation can be achieved with diverse stimuli. Such a programmable self-propelling actuator provides a vivid counterpart to bacteria and markedly extends our understanding of the rotation-translation conversion performed in an exquisite self-organized system. In addition to the controllable trajectory, motions of loaded particles are also found to be sensitive to their surface energy and geometries. This may pave a new way for intelligent manufacturing and optofluidics and will inspire fantastic applications in microassembly lines and automatic sorters. Also, the semi-free system is compatible with fluorescence biosensing techniques, thus facilitating lab-on-a-chip diagnostics and immunoassays.

In conclusion, we propose a strategy for programmable self-propelling actuators via architecting the exquisite configuration of a photoresponsive helical medium. The light-driven winding/unwinding of CLC helix works as a motor, and it laterally transports sputtered microspheres with a self-organized microstructure-engaged transmission system. Via rationally preprogramming the alignment condition, functional actuators that can massively and parallelly transport microspheres in customized trajectories are demonstrated. Such a stimuli-responsive and microstructure-engaged system mimics the motion of bacteria and provides a new insight into the relationship between the function and the structure evolution. This work supplies a platform for versatile self-propelling microactuators and paves a bright way toward smart materials, intelligent robots, micro/nanoassembling, cargo transport, and manufacturing.

MATERIALS AND METHODS

Materials

The photoresponsive CLC was mixed by 1.0 weight % (wt %) left-handed chiral molecular switch ChAD-3c-S (BEAM, USA) and 99.0 wt % nematic LC host E7 (Jiangsu Hecheng Display Technology Co., Ltd., China). The absorption spectra of ChAD-3c-S is shown in fig. S13. The initial HTP is about $-42.6\ \mu m^{-1}$, and a green light–stabilized HTP is about $-30.7\ \mu m^{-1}$ (*39*). A polarization-sensitive sulfonic azo dye SD1 (Dai-Nippon Ink and Chemicals, Japan; fig. S14) was dissolved in *N*,*N*′-dimethylformamide at a concentration of 0.3 wt % and then spin-coated as a photoalignment film. It reorients the absorption oscillator to be perpendicular to the incident polarization. Methacrylate-resin microspheres with a diameter of 3 μm (EPOSTAR, Japan) were used to explore the rotation-translation conversion (fig. S15), which induce tangential anchoring to surrounding LCs (fig. S16).

Sample fabrication

Glass substrates were ultrasonically bathed, ultraviolet ozone–cleaned (30 min), and then spin-coated with SD1 solution (3000 rpm). After curing at 100°C for 10 min to evaporate the solvent, the substrates were positioned at the image plane of the Digital Micro-mirror Device-based microlithography system (*40*). For unidirectional photoalignment, a uniform exposure with linear-polarized blue light (450 nm) was carried out. The designed alignment patterns were generated via a multistep partly overlapping exposure process with a synchronous polarization control. Then, the CLC was heated to 70°C and spin-coated on the photoaligned substrate at 1000 rpm for 30 s. The photoalignment pattern dominates the local director orientation thanks to the strong anchoring energy of SD1, thus suppressing the shear-induced alignment (fig. S17). Then, the samples were placed in a box horizontally. About 1 mg of dry microparticles was sputtered by a nitrogen flow (0.2 MPa) and then gently distributed onto the semi-free films by the gravity. Five minutes later, the samples were taken out for characterizations.

Characterization

The melting point and clearing point were measured by a differential scanning calorimetry (Mettler-Toledo DSC1 STARe), which were −60°

and 58°C, respectively (fig. S18). A spectral interferometric method for film thickness measurement was described in text S3. All the samples were examined at room temperature under ambient environment. The textures of fingerprint patterns were observed under a POM (Nikon Eclipse 50i Pol) in the transmission mode with a pair of crossed polarizers and recorded by a charge-coupled device camera (Nikon DS-U3). The blue light–stimulating process was performed under the reflection mode of POM through a bandpass filter (450 to 490 nm). The irradiance of blue light was about 100 $\mu W/cm^2$. The green light exposure process was carried out with an LED light source at 530 nm with the irradiance of 1 mW/cm^2. The experimental setup is shown in fig. S19. The diffraction was performed with a He-Ne laser at 632.8 nm, and diffraction patterns were captured by a digital camera (Canon EOS 600D). A fluorescence confocal microscopy (Olympus FV3000) was used to observe the location of microspheres. We used a 561-nm laser beam to excite the dye, and the detection range was 600 to 650 nm. The CLC was doped with a fluorescent dye (rhodamine B, 0.02 wt %; emission peak, 625 nm) for the above measurement.

SUPPLEMENTARY MATERIALS

Supplementary material for this article is available at http://advances.sciencemag.org/cgi/content/full/7/32/eabh3505/DC1

REFERENCES AND NOTES

1. C. Peng, T. Turiv, Y. Guo, Q.-H. Wei, O. D. Lavrentovich, Command of active matter by topological defects and patterns. *Science* **354**, 882–885 (2016).
2. Y. Chang, K. Zhang, B. L. Carroll, X. Zhao, N. W. Charon, S. J. Norris, M. A. Motaleb, C. Li, J. Liu, Molecular mechanism for rotational switching of the bacterial flagellar motor. *Nat. Struct. Mol. Biol.* **27**, 1041–1047 (2020).
3. E. J. Cohen, J. L. Ferreira, M. S. Ladinsky, M. Beeby, K. T. Hughes, Nanoscale-length control of the flagellar driveshaft requires hitting the tethered outer membrane. *Science* **356**, 197–200 (2017).
4. D. Chen, Q. Pei, Electronic muscles and skins: A review of soft sensors and actuators. *Chem. Rev.* **117**, 11239–11268 (2017).
5. T. J. White, D. J. Broer, Programmable and adaptive mechanics with liquid crystal polymer networks and elastomers. *Nat. Mater.* **14**, 1087–1098 (2015).
6. M. Duduta, E. Hajiesmaili, H. Zhao, R. J. Wood, D. R. Clarke, Realizing the potential of dielectric elastomer artificial muscles. *Proc. Natl. Acad. Sci. U.S.A.* **116**, 2476–2481 (2019).
7. W. Feng, D. J. Broer, D. Liu, Oscillating chiral-nematic fingerprints wipe away dust. *Adv. Mater.* **30**, 1704970 (2018).
8. A. H. Gelebart, D. Jan Mulder, M. Varga, A. Konya, G. Vantomme, E. W. Meijer, R. L. B. Selinger, D. J. Broer, Making waves in a photoactive polymer film. *Nature* **546**, 632–636 (2017).
9. X. Lu, S. Guo, X. Tong, H. Xia, Y. Zhao, Tunable photocontrolled motions using stored strain energy in malleable azobenzene liquid crystalline polymer actuators. *Adv. Mater.* **29**, 1606467 (2017).
10. B. Zuo, M. Wang, B.-P. Lin, H. Yang, Visible and infrared three-wavelength modulated multi-directional actuators. *Nat. Commun.* **10**, 4539 (2019).
11. S. Iamsaard, S. J. Aßhoff, B. Matt, T. Kudernac, J. J. L. M. Cornelissen, S. P. Fletcher, N. Katsonis, Conversion of light into macroscopic helical motion. *Nat. Chem.* **6**, 229–235 (2014).
12. Y. Yu, M. Nakano, T. Ikeda, Photomechanics: Directed bending of a polymer film by light. *Nature* **425**, 145 (2003).
13. Z.-C. Jiang, Y.-Y. Xiao, Y. Zhao, Shining light on liquid crystal polymer networks: Preparing, reconfiguring, and driving soft actuators. *Adv. Opt. Mater.* **7**, 1900262 (2019).
14. Z. Zou, N. Clark, Pumping liquid crystals. *Phys. Rev. Lett.* **75**, 1799–1802 (1995).
15. X. Wang, D. S. Miller, E. Bukusoglu, J. J. de Pablo, N. L. Abbott, Topological defects in liquid crystals as templates for molecular self-assembly. *Nat. Mater.* **15**, 106–112 (2016).
16. S. S. Lee, J. B. Kim, Y. H. Kim, S.-H. Kim, Wavelength-tunable and shape-reconfigurable photonic capsule resonators containing cholesteric liquid crystals. *Sci. Adv.* **4**, eaat8276 (2018).
17. C. Blanc, Colloidal crystal ordering in a liquid crystal. *Science* **352**, 40–41 (2016).
18. C.-l. Yuan, W. Huang, Z.-g. Zheng, B. Liu, H. K. Bisoyi, Y. Li, D. Shen, Y. Lu, Q. Li, Stimulated transformation of soft helix among helicoidal, heliconical, and their inverse helices. *Sci. Adv.* **5**, eaax9501 (2019).
19. A. Kausar, H. Nagano, T. Ogata, T. Nonaka, S. Kurihara, Photocontrolled translational motion of a microscale solid object on azobenzene-doped liquid-crystalline films. *Angew. Chem. Int. Ed.* **48**, 2144–2147 (2009).
20. Y. Guo, S. Afghah, J. Xiang, O. D. Lavrentovich, R. L. B. Selinger, Q. H. Wei, Cholesteric liquid crystals in rectangular microchannels: Skyrmions and stripes. *Soft Matter* **12**, 6496 (2016).
21. F. Serra, S. Yang, Liquid crystals: Material defect lines. *Nat. Mater.* **15**, 10–11 (2015).
22. L. Tran, K. J. M. Bishop, Swelling cholesteric liquid crystal shells to direct the assembly of particles at the interface. *ACS Nano* **14**, 5459–5467 (2020).
23. S. Bono, S. Sato, Y. Tabe, Unidirectional rotation of cholesteric droplets driven by UV-light irradiation. *Soft Matter* **13**, 6569–6575 (2017).
24. M. Rajabi, H. Baza, T. Turiv, O. D. Lavrentovich, Directional self-locomotion of active droplets enabled by nematic environment. *Nat. Phys.* **17**, 260–266 (2021).
25. L. Tran, H.-N. Kim, N. Li, S. Yang, K. J. Stebe, R. D. Kamien, M. F. Haase, Shaping nanoparticle fingerprints at the interface of cholesteric droplets. *Sci. Adv.* **4**, eaat8597 (2018).
26. Z.-G. Zheng, Y. Li, H. K. Bisoyi, L. Wang, T. J. Bunning, Q. Li, Three-dimensional control of the helical axis of a chiral nematic liquid crystal by light. *Nature* **531**, 352–356 (2016).
27. R. Eelkema, M. M. Pollard, J. Vicario, N. Katsonis, B. S. Ramon, C. W. M. Bastiaansen, D. J. Broer, B. L. Feringa, Molecular machines: Nanomotor rotates microscale objects. *Nature* **440**, 163 (2006).
28. A. Ryabchun, A. Bobrovsky, Cholesteric liquid crystal materials for tunable diffractive optics. *Adv. Opt. Mater.* **6**, 1800335 (2018).
29. R. Eelkema, M. M. Pollard, N. Katsonis, J. Vicario, D. J. Broer, B. L. Feringa, Rotational reorganization of doped cholesteric liquid crystalline films. *J. Am. Chem. Soc.* **128**, 14397–14407 (2006).
30. L.-L. Ma, W. Duan, M.-J. Tang, L.-J. Chen, X. Liang, Y.-Q. Lu, W. Hu, Light-driven rotation and pitch tuning of self-organized cholesteric gratings formed in a semi-free film. *Polymers* **9**, 295 (2017).
31. I. I. Smalyukh, O. D. Lavrentovich, Three-dimensional director structures of defects in Grandjean-Cano wedges of cholesteric liquid crystals studied by fluorescence confocal polarizing microscopy. *Phys. Rev. E* **66**, 051703 (2002).
32. A. Eremin, P. Hirankittiwong, N. Chattham, H. Nádasi, R. Stannarius, J. Limtrakul, O. Haba, K. Yonetake, H. Takezoe, Optically driven translational and rotational motions of microrod particles in a nematic liquid crystal. *Proc. Natl. Acad. Sci. U.S.A.* **112**, 1716–1720 (2015).
33. K. Nayani, A. A. Evans, S. E. Spagnolie, N. L. Abbott, Dynamic and reversible shape response of red blood cells in synthetic liquid crystals. *Proc. Natl. Acad. Sci. U.S.A.* **117**, 26083–26090 (2020).
34. H. Mundoor, B. Senyuk, I. I. Smalyukh, Triclinic nematic colloidal crystals from competing elastic and electrostatic interactions. *Science* **352**, 69–73 (2016).
35. J. S. Lintuvuori, A. C. Pawsey, K. Stratford, M. E. Cates, P. S. Clegg, D. Marenduzzo, Colloidal templating at a cholesteric-oil interface: Assembly guided by an array of disclination lines. *Phys. Rev. Lett.* **110**, 187801 (2013).
36. J. C. Loudet, P. Hanusse, P. Poulin, Stokes drag on a sphere in a nematic liquid crystal. *Science* **306**, 1525 (2004).
37. O. D. Lavrentovich, Transport of particles in liquid crystals. *Soft Matter* **10**, 1264–1283 (2014).
38. M. Yada, J. Yamamoto, H. Yokoyama, Direct observation of anisotropic interparticle forces in nematic colloids with optical tweezers. *Phys. Rev. Lett.* **92**, 185501 (2004).
39. Y.-C. Hsiao, K.-C. Huang, W. Lee, Photo-switchable chiral liquid crystal with optical tristability enabled by a photoresponsive azo-chiral dopant. *Opt. Express* **25**, 2687–2693 (2017).
40. L.-L. Ma, S.-S. Li, W.-S. Li, W. Ji, B. Luo, Z.-G. Zheng, Z.-P. Cai, V. Chigrinov, Y.-Q. Lu, W. Hu, L.-J. Chen, Rationally designed dynamic superstructures enabled by photoaligning cholesteric liquid crystals. *Adv. Opt. Mater.* **3**, 1691–1696 (2015).
41. J. Baudry, M. Brazovskaia, L. Lejcek, P. Oswald, S. Pirkl, Arch-texture in cholesteric liquid crystals. *Liq. Cryst.* **21**, 893–901 (1996).
42. N. Hijnen, T. A. Wood, D. Wilson, P. S. Clegg, Self-organization of particles with planar surface anchoring in a cholesteric liquid crystal. *Langmuir* **26**, 13502–13510 (2010).

Acknowledgments: We appreciate Q.-H. Wei, B.-X. Li, G.-H. Wang, Y. Ding, L.-L. Li, H. Qian, D.-L. Wang, W. Zhang, Y. Liu, and K.-H. Wu for constructive discussions and valuable help. **Funding:** This work was supported by the National Key Research and Development Program of China (2017YFA0303700 to Y.-Q.L.), National Natural Science Foundation of China (NSFC) (62035008 and 61922038 to W.H., 52003115 to L.-L.M., and 12004175 to P.C.), Natural Science Foundation of Jiangsu Province (BK20200320 to L.-L.M. and BK20200311 to P.C.), Fundamental Research Funds for the Central Universities (021314380189 to W.H.), and Innovation and Entrepreneurship Program of Jiangsu Province. **Author contributions:** W.H. and L.-L.M. conceived the original idea and designed the experiment. L.-L.M. and C.L. prepared the

samples and performed the experiments. L.-L.M., C.L., W.H., S.-B.W., P.C., Q.-M.C., J.-X.Q., S.-J.G., and Y.-H.W. analyzed the experimental data. L.-L.M., W.H., and C.L. prepared the initial manuscript with the assistance of Y.-Q.L., S.-B.W., and Q.-M.C. All authors participated in the discussion and contributed to refining the manuscript. W.H. and Y.-Q.L. co-supervised and directed the research. **Competing interests:** The authors declare that they have no competing interests. **Data and materials availability:** All data needed to evaluate the conclusions in the paper are present in the paper and/or the Supplementary Materials. Additional data related to this paper may be requested from the authors.

Submitted 3 March 2021
Accepted 17 June 2021
Published 6 August 2021
10.1126/sciadv.abh3505

Citation: L.-L. Ma, C. Liu, S.-B. Wu, P. Chen, Q.-M. Chen, J.-X. Qian, S.-J. Ge, Y.-H. Wu, W. Hu, Y.-Q. Lu, Programmable self-propelling actuators enabled by a dynamic helical medium. *Sci. Adv.* **7**, eabh3505 (2021).

Science Advances

Programmable self-propelling actuators enabled by a dynamic helical medium

Ling-Ling Ma, Chao Liu, Sai-Bo Wu, Peng Chen, Quan-Ming Chen, Jia-Xin Qian, Shi-Jun Ge, Yuan-Hang Wu, Wei Hu and Yan-Qing Lu

Sci Adv **7** (32), eabh3505.
DOI: 10.1126/sciadv.abh3505